Article published online: 2021-04-08

Serum Pharmacochemistry Analysis Combined with Network Pharmacology Approach to Investigate the Antiosteoporosis Effect of Xianlinggubao Capsule *in vivo*

Yun-Hui Xu[1#] Yi-Chun Sun[2,3#] Jie Liu[1] Hui-Xin Li[2] Chun-Yue Huang[1] Yuan-Yuan Pang[2] Tong Wu[1*] Xiao Hu[1,2*]

[1] State Key Lab. of New Drug and Pharmaceutical Process, Shanghai Institute of Pharmaceutical Industry, China State Institute of Pharmaceutical Industry, Shanghai, People's Republic of China
[2] Sinopharm Group Tongjitang (Guizhou) Pharmaceutical Co., Ltd., Guiyang, People's Republic of China
[3] Guangdong Efong Pharmaceutical Co., Ltd, Guangzhou, People's Republic of China

Address for correspondence Xiao Hu, Shanghai Institute of Pharmaceutical Industry, 285 Gebaini Road, Shanghai 201203, People's Republic of China (e-mail: xjtuyxhx@126.com).

Tong Wu, Shanghai Institute of Pharmaceutical Industry, 285 Gebaini Road, Shanghai 201203, People's Republic of China (e-mail: tongwu88@163.com).

Pharmaceut Fronts 2020;2:e168–e178.

Abstract

Xianlinggubao capsule (XLGB) is a traditional Chinese medicine multi-component herbal prescription and has been widely used in osteoporosis (OP) treatment. However, the underlying anti-OP mechanisms of XLGB have not been fully studied. In this study, an ovariectomized rat model of OP was established. The OP rats were orally administrated with XLGB, and then the main absorbed components in serum sample were assessed based on liquid chromatography-tandem mass spectrometry (LC-MS/MS). Subsequently, the potential anti-OP markers in XLGB were screened based on a network pharmacology strategy. Molecular docking analysis was used for confirmation. LC-MS showed 22 absorbed components in the serum sample of OP rat with XLGB treatment. Network pharmacology and pathway analysis suggested 19 potential anti-OP markers in XLGB. According to molecular docking process, most of the potential markers displayed strong interactions with the 22 absorbed components mentioned above. Besides, an absorbed component–potential marker–pathway network was further established. In conclusion, our data suggested the possible mechanisms for XLGB in OP treatment, in which the "multicomponents, multitargets, and multipathways" participated. Our article provided possible direction for drug discovery in OP and could help for exploring novel application of XLGB in clinical setting.

Keywords
- xianlinggubao capsule
- osteoporosis
- mechanism
- serum pharmacochemistry analysis
- network pharmacology
- molecular docking

Introduction

Osteoporosis (OP) is a complex bone disorder with a genetic background, and is characterized by progressive deterioration in bone tissue, which results in a decrease in bone mass, quality, and strength, and an increase in bone fracture risk.[1,2] It has been estimated that the number of annual OP-related fractures in the United States will increase from 2 to 3 million in the period from 2005 to 2025, and the associated acute and long-term medical care cost will increase from $17 billion to $25 billion.[3] The prevalence and high medical costs of OP also remain true in developing countries including China. According to epidemiological investigation, China's OP incidence rate in 2008 was 14.94%; however, during 2012 to

[#] *These authors contributed equally to this work.*

received
December 28, 2020
accepted
February 10, 2021
published online
April 8, 2021

DOI https://doi.org/10.1055/s-0041-1726301.
ISSN 2628-5088.

Georg Thieme Verlag KG, Rüdigerstraße 14, 70469 Stuttgart, Germany

2015, it increased up to 27.96%,[4] with, the direct medical costs of hip fracture in 2006 reaching approximately US$ 1.5 billion.[5] It is obvious that with the rapid increase in aging population, OP incidence in developing countries will increase more and more significantly in the future. Evidence suggests that by 2050, the number of hip fractured in Asia will be increase by 50%.[6,7] Given above, OP is a growing global public health problem with substantial medical, social, and economic burden.

Chinese herbal medicines play an important role in the preclinical and clinical studies of OP.[8] Xianlinggubao formula was designed based on modification of the empirical "Miao minority" medicine, which was commonly used to tone the "kidney system" and nourish bones. Xianlinggubao capsule (XLGB) was officially approved and sold as the over-the-counter (OTC) drug in China (CFDA, Z20025337). It is the only traditional Chinese medicine (TCM) prescription that was used for the prevention and treatment of OP on the National Health Insurance List in China. Its safety and efficacy have been proven by the principle of evidence-based medicine.[9] Preclinical studies showed that XLGB could improve bone mineral density and mechanical strength in ovariectomized (OVX)-induced OP in old rats.[10] However, the active compounds and the underlying mechanism of XLGB have not been fully understood.

As a TCM Fufang (multi-component) prescription, XLGB consists of six commonly used Chinese herbs with their percentages in weight as follows: *Herba Epimedii* (*Epimedium brevicornu* Maxim, Yinyanghuo) (70%), *Radix Dipsaci* (root of *Dipsacus asper Wall* ex Henry, Xuduan) (10%), *Rhizoma Anemarrhenae* (rhizome of *Anemarrhena asphodeloides* Bunge, Zhimu) (5%), *Radix et Rhizoma Salviae* (root and rhizome of *Salvia miltiorrhiza* Bunge, Danshen) (5%), *Fructus Psoraleae* (fruit of *Psoralea corylifolia* L., Buguzhi) (5%), and *Radix Rehmanniae* (root of *Rehmannia glutinosa* Libosch, Dihuang) (5%).[11] Chemical analysis showed that there are a large number of compounds with different structures in this formula,[12] which makes the study of the anti-OP mechanism of XLGB a great challenge. In 2020, Bao et al used the network pharmacology, a popular method for investigating the underlying molecular mechanisms for TCM in recent years, to systematically study the possible therapeutic mechanisms of XLGB in OP.[13,14] It is well known that XLGB, an oral medicine, plays roles only if it is absorbed into the blood, thus, investigating the anti-OP mechanisms of XLGB at the molecular and system levels *in vivo* remains urgent.

In this study, we identified absorbed compounds of XLGB in the serum sample of OVX rats through a pharmacochemistry test. Potential markers were screened by network pharmacology analysis based on protein–protein interaction (PPI) data and KEGG (Kyoto Encyclopedia of Genes and Genomes) enrichment. Molecular docking was employed to investigate the strength of interaction between absorbed components and potential markers. Furthermore, an absorbed component–potential marker–pathway network was established. The detailed flowchart of this work is depicted in ►**Fig. 1**. Our data first and systematically demonstrated the therapeutic mechanisms XLGB in an *in vivo* study.

Materials and Methods

Serum Pharmacochemistry Analysis of XLGB

Establishment and Treatment of OVX-Induced OP in Rats

Female Sprague–Dawley rats (200–220 g) were anesthetized with pentobarbital sodium (40 mg/kg, intraperitoneal), and their ovaries were removed bilaterally. Thirty days later, the indexes of bone density were measured by X-ray absorptiometry. Serum concentrations of osteocalcin, N-terminal propeptide of type I procollagen (PINP), alkaline phosphatase (ALP), and tartrate resistant acid phosphatase (TRAP) were estimated using an enzyme-linked immunosorbent assay kit following the reported study to assess the successful establishment of OVX-induced OP in rat models.[15–17]

OVX rats were divided into two groups: XLGB and control groups. Rats in the XLGB group ($n = 5$) were intragastrically treated with XLGB (300 mg/kg daily, Lot No. 1611016, GuizhouTongji Tang Pharmaceutical Co., Ltd.) for 50 consecutive days. Rats in the control group ($n = 5$) were treated with physiological saline in the same way as that in the XLGB group. All experiments were approved by the Laboratory Animal

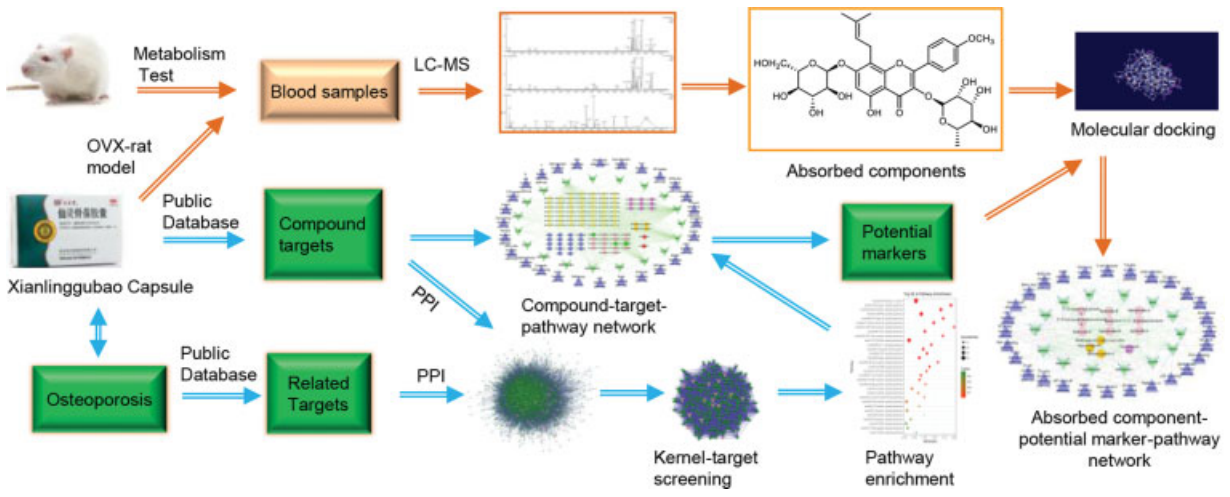

Fig. 1 The flowchart of network pharmacology approach.

Ethics Committee of Shanghai Institute of Pharmaceutical Industry.

Identification of the Absorbed Components

On the 50th day, all rats were anesthetized by intraperitoneal injection of 10% aqueous chloral hydrate. After 2 hours, the blood samples from the hepatic portal vein were collected, centrifuged at 14,000 rpm for 15 minutes at 4°C, and then mixed to produce the pooled plasma.

Serum pharmacochemistry analysis was performed on a Waters UPLC (ultra-performance liquid chromatography) system using an ACQUITY UPLCHSS T3 column (2.1×100 mm, 1.7 µm) with a security guard column of the same material at a flow rate of 0.4 mL/minute. The mobile phases A and B were 0.1% formic acid in water and acetonitrile, respectively. The gradient program was as follows: 0–0.15 minutes, 98% A; 0.15–17.34 minutes, 98–69% A; 17.34–20.78 minutes, 69–52% A; 20.78–24.22 minutes, 52–20% A; 24.22–26.00 minutes, 20–0% A, 26.00–29.00 minutes, 0% A; 29.00–29.10 minutes, 0–2% A; 32.5 minutes, 2% A. UV spectra from 190 to 400 nm were recorded online.

Mass spectra were acquired in both positive and negative ion modes by using a Waters definition accurate mass quadrupole time-of-flight (Q-TOF) Xevo G2-XS mass spectrometer (Waters MS Technologies, United Kingdom) equipped with an electrospray ionization source. The optimized operating parameters were set as follows: mass range, *m/z*: 50–1,500; the flow rate of drying gas (N_2): 800 L/h; drying gas temperature: 400°C; cone gas flow: 100 L/h; source temperature: 120°C; capillary voltage: 2.5 kV; cone voltage: 40 V; in MSE mode, the energies for collision induced dissociation were 6 V for the precursor ion at low energy mode and 30 to 60 V for fragmentation information at high energy mode. An external reference (Lock-Spray) consisting of a 0.2 ng/mL solution of leucine enkephalin was used in both positive (*m/z*: 556.2771 $[M + H]^+$) and negative modes (*m/z*: 554.2615 $[M - H]^-$), infused at a flow of 5 µL/minute. All the data were acquired using MassLynx 4.1 software (Waters, Milford, Massachusetts, United States).

Potential Marker Screening

Composite Compounds and ADME (Absorption, Distribution, Metabolism, Excretion) Screening of XLGB

The chemical composition of all the six herbs of XLGB was obtained from the Traditional Chinese Medicine System Pharmacology Database (TCMSP, http://lsp.nwu.edu.cn/tcmsp.php) and TCM database@Taiwan (http://tcm.cmu.edu.tw/index.php). Pharmacokinetic properties of each compound, including the prediction of oral bioavailability (OB), intestinal epithelial permeability (Caco-2 cells), drug likeness (DL), blood–brain barrier (BBB), drug half-life, and Lipinski's rule (LR) of five[18] were assessed for screening and evaluation of the target compounds. The selected candidate molecules should satisfy the criteria: OB $\geq$ 30%, DL $\geq$ 0.18, Caco-2 > -0.40, suggested by the TCMSP database[19] and LR of five. Besides, to discover the active ingredients as much as possible, we searched a large number of texts and selected some main ingredients of these herbs or compounds with pharmacological activity in our prescreening process to supplement the compound library.

Compound Targets for XLGB

The potential targets of the predicted active compounds of XLGB were explored from TCMSP. Besides, SWISS database (http://www.swisstargetprediction.ch), STITCH database (http://stitch.embl.de), and target prediction system (https://prediction.charite.de/subpages/target_prediction.php) were further used for prediction for those that failed to be collected in TCMSP. UniProt (http://www.uniprot.org/) serves as a central hub for the collection of functional information on proteins, and has the advantages of accurate, consistent, and rich annotation. In this study, UniProt was applied to resolve nonstandard naming.

Candidate Targets for OP

OP-related targets were collected using "Osteoporosis" as the keyword from four existing resources, namely, Online Mendelian Inheritance in Man database (OMIM; http://www.omim.org/), Genetic Association Database (GAD; http://geneticassociationdb.nih.gov/), Therapeutic Target Database (TTD; http://db.idrblab.net/ttd/), and pharm-GKB (https://www.pharmgkb.org/). The official gene symbols were acquired through UniProt translation.

Kernel Targets for XLGB against OP

System biology studies show that genes and proteins are interconnected and the PPI networks are usually used to understand the role of various proteins in complex diseases. PPI data can be obtained using the Cytoscape plugin Bisogenet. In this study, the intersection of compound target PPI data and OP target PPI data was established to study the anti-OP effect of compounds, and the kernel targets were screened with node degree and Cytoscape plugin CytoNCA.

Enrichment Analysis and Potential Target Screening

The Database for Annotation, Visualization and Integrated Discovery (DAVID; https://david-d.ncifcrf.gov, ver. 6.8) was applied.[20] Pathway enrichment was performed through inputting the kernel genes into DAVID.

Molecular Docking

The structure of the absorbed compounds was downloaded from PubChem (https://pubchem.ncbi.nlm.nih.gov/). In this study, three-dimensional structures of the 19 target peptides were derived from the RCSB Protein Data Bank (http://www.rcsb.org/pdb/home/home.do). The docking calculation was performed using the software DOCK (6.7) on Yinfo Cloud Computing Platform, a 6 server for biomedicinal, material, and statistical researches (http://cloud.yinfotek.com).[21] The best ranked docking pose of the peptide in the active site of each compound was determined according to the grid scores.

Network Construction

All the networks can be created via utilizing the network visualization software Cytoscape (http://cytoscape.org/, ver.

3.4.0).[22] This is a software that applies to visualizing biological pathways, intermolecular interaction networks, etc. Meanwhile, it also supplies a basic set of features for data integration, analysis, and visualization for complicated network analysis.

Results

Pharmacochemistry Analysis of XLGB in Serum Sample of OP Rats

Successful Establishment of OVX Model of OP in Rats

In this article, the OVX-induced OP model in rat was established. ►**Fig. 2** shows that bone density and osteocalcin in model rats decreased significantly ($p < 0.05$ and $p < 0.01$ vs. normal, respectively), while serum levels of PINP, ALP, and TRAP increased significantly ($p < 0.01$ vs. normal), demonstrating the successful establishment of the OVX model of OP in rats.

Identification of the Absorbed Components

According to the UPLC-QTOF MS analysis, 22 prototype components were identified from OVX rat plasma after oral administration of XLGB (►**Fig. 3** and ►**Table 1**).

Potential Target Screening

Candidate Compound Screening for XLGB

A total of 520 ingredients were obtained from TCMSP, and 83 candidate compounds were retained after LR and ADME screening; 28 compounds of *Fructus Psoraleae* were gained from TCM database@Taiwan. In addition, 15 compounds, either with extensive pharmacological activities or were the typical components of six herbs but failed to meet LR or the ADME criteria, have been supplemented. In total, 126 candidate compounds were determined and are listed in ►**Supplementary Table S1** (online only).

Identification of Common Targets for XLGB against OP

A total of 328 putative targets for 124 candidate compounds were collected from the aforementioned database, while 285 OP-related targets were collected, of which 94, 215, 10, and 24 from OMIM, GAD, pharm-GKB, and TTD, respectively.

Pathway Enrichment for Kernel Targets and Potential Marker Screening

First, an intersected network was constructed between a compound putative target PPI network and an OP-related target PPI network to unravel the pharmacological mechanisms of XLGB against OP. Further, based on the plugin named CytoNCA,[23] 343 kernel targets were identified. We then input all kernel targets into the DAVID to enrich OP-associated pathways, and 31 pathways with $p \leq 0.05$ were obtained. They were performed using the OmicShare tools (http://www.omicshare.com/tools) and are shown in ►**Fig. 4**.

The 31 pathways containing 104 of the 343 targets might be the key pathways for the anti-OP mechanism of XLGB. Comparing the kernel targets of the pathway with the targets of 124 candidate compounds, we found that 19 kernel targets were overlapped (►**Table 2**), which might be considered as

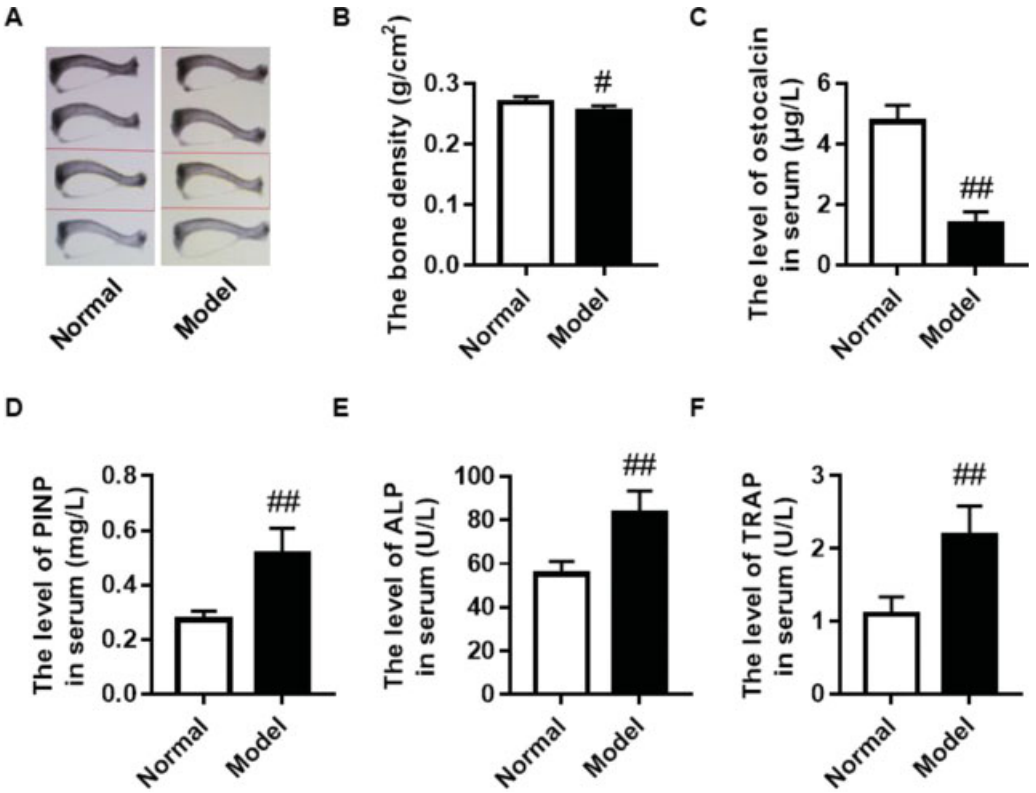

Fig. 2 Comparison of (**A** and **B**) bone density, and serum sample of (**C**) osteocalcin, (**D**) PINP, (**E**) ALP, and (**F**) TRAP between the model group and the normal control group. $^{\#}p < 0.05$; $^{\#\#}p < 0.01$ versus normal. ALP, alkaline phosphatase; PINP, propeptide of type I procollagen; TRAP, tartrate resistant acid phosphatase.

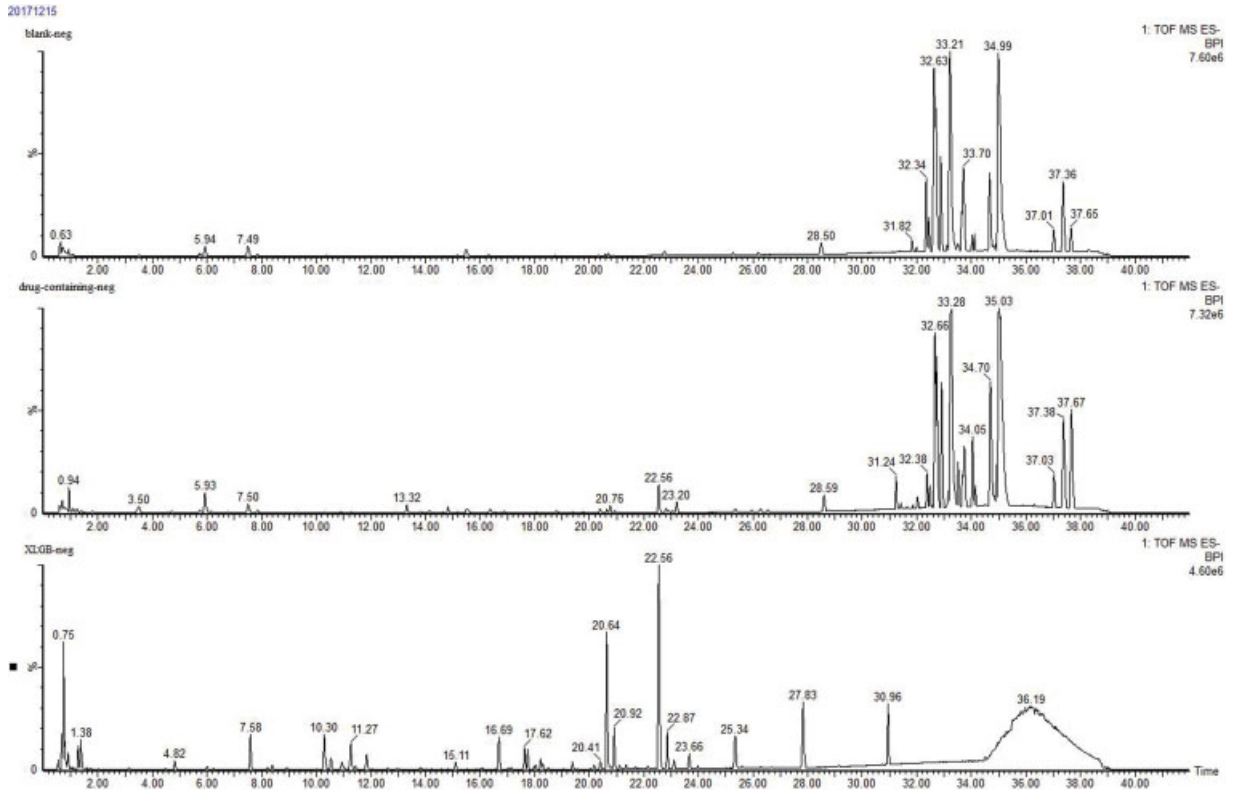

Fig. 3 LC-MS spectra demonstrating the pharmacochemistry analysis in the serum sample of OVX model of OP rat. LC-MS, liquid chromatography–mass spectrometry; OP, osteoporosis; OVX, ovariectomized.

potential markers and will function in the anti-OP process of XLGB.

Then, a compound–target–pathway network was constructed as shown in ►**Fig. 5**, in which 105 compounds from six herbs of XLGB (►**Supplementary Table S1**, online only) acted on 28 pathways (►**Table 3**) through 19 potential markers.

Interaction between Potential Markers and Absorbed Compounds

Docking Results

Molecular docking analysis was performed to investigate the interaction between the 22 absorbed compounds and 19 potential markers. Proteins without detected crystal structures were excluded from the analysis. Grid scores of the docking results are showed in ►**Supplementary Table S2** (online only). Grid scores less than −80 kcal/mol were considered to be strong interaction. Our article suggested 14 potential markers with 13 absorbed components, among which 9 absorbed components were from *Herba Epimedii*, 3 absorbed components were from *Radix Dipsaci*, and 1 absorbed component was from *Rhizoma Anemarrhenae*.

Absorbed Component–Potential Marker–Pathway Network

A network was constructed to show the interaction among main absorbed components, potential markers, and pathways. ►**Fig. 6** demonstrates 13 absorbed components acted on 14 potential targets that connected to 28 pathways.

Discussion

It is well known that compounds will function on the premise that they are absorbed into the body. Thus, in this study, we investigated the interaction between screened potential markers and absorbed components to illuminate the anti-OP effect of XLGB in an *in vivo* study.

The clinical specification of XLGB is 0.5 g/piece following the instructions described. Adults take three pieces every time, twice a day. We first suggested an oral dose of 300 mg/kg/day of XLGB for an OVX rat model of OP, which was equivalent to the corresponding clinical prescription dose for a 60 kg human subject and would make sure the results of our research study are as close as possible to clinical use. Then, we identified 22 main prototype components of XLGB in the serum sample of an OVX rat model of OP. This number was smaller than that given in Geng et al's report based on a healthy mice[24] (57 prototype components). This may be resulted from animals in different conditions (normal and pathological). The TCM theory supports that the monarch and minister drugs may play a major role in a fufang prescription. In this article, we found that 11 of the 22 compounds are from *Herba Epimedii* (a monarch drug in the prescription), 7 from *Radix Dipsaci*, and 3 from *Fructus Psoraleae*, both of which are the minister drugs of XLGB.

The PPI networks were applied to investigate the relationship between compound targets and disease genes. We screened our potential markers based on network pharmacology analysis with PPI data and the enrichment analysis of KEGG pathways. We suggested a total of 124 candidate active

Table 1 LC–MS data of 22 absorbed prototype compounds from OVX rat plasma after oral administration of XLGB

t_R/min	Selected ion	Measured mass	MS/MS fragmentation	Identification	Source
7.58	$[M-H]^-$	375.1281	421.1342, 375.1281, 213.0746	Loganic acid[b,c]	*Radix Dipsaci*
10.30	$[M+HCOO]^-$	403.1233	403.1233, 197.8060	Sweroside[b,c]	*Radix Dipsaci*
10.54	$[M+HCOO]^-$	435.1495	435.1495	Loganin[b,c]	*Radix Dipsaci*
11.03	$[M+HCOO]^-$	583.2044	583.2044	Olivil-4′′-O-β-D-glucopyranoside[b,c]	*Herba Epimedii*
11.26	$[M-H]^-$	365.0866	365.0866, 159.0431	Psoralenoside[b]	*Fructus Psoraleae*
11.84	$[M-H]^-$	365.0872	365.0872, 159.0436	Isopsoralenoside[b]	*Fructus Psoraleae*
12.64	$[M-H]^-$	563.1424	563.1424	Kaempferol 3-O-xylosyl-(1→2)–rhamnoside[b]	*Herba Epimedii*
17.76	$[M-H]^-$	823.2709	823.2709, 661.2162, 352.0941	Diphylloside A[b]	*Herba Epimedii*
17.99	$[M-H]^-$	793.2575	793.2575, 631.2067	3′′-O-Xylopyranosyl epimedoside A[b]	*Herba Epimedii*
18.22	$[M-H]^-$	807.2759	807.2759, 645.2204, 351.0852	Diphylloside B[b]	*Herba Epimedii*
19.39	$[M-H]^-$	919.5035	965.5030, 919.5035, 757.4406, 595.3853	Timosaponin B-II[a]	*Rhizoma Anemarrhenae*
20.17	$[M+HCOO]^-$	883.2924	883.2924, 675.2317, 366.1105	Epimedin A[a]	*Herba Epimedii*
20.41	$[M+HCOO]^-$	853.2797	853.2797, 645.2215, 366.1105	Epimedin B[a]	*Herba Epimedii*
20.64	$[M+HCOO]^-$	867.2959	867.2959, 857.2675, 821.2942, 659.2356, 366.1093	Epimedin C[a]	*Herba Epimedii*
20.92	$[M+HCOO]^-$	721.2374	721.2374, 367.1163	Icariin[a]	*Herba Epimedii*
22.56	$[M-H]^-$	927.4996	973.50481, 927.4996, 603.39049, 323.0965	Asperosaponin VI[a]	*Radix Dipsaci*
25.34	$[M-H]^-$	795.4637	841.4637, 795.4637, 645.4028, 471.3474	Hederagenin β-sophorosyl ester[b]	*Radix Dipsaci*
27.83	$[M-H]^-$	659.2362	659.2362, 366.1090, 351.0863	2′′-O-Rhamnosylicariside II[a]	*Herba Epimedii*
29.15	$[M-H]^-$	513.17767	513.17767	Icariside II[a]	*Herba Epimedii*
29.53	$[M-H]^-$	911.50419	957.5141, 911.50419, 749.4536, 603. 3957	Akebia saponin V[b]	*Radix Dipsaci*
30.96	$[M+HCOO]^-$	603.3915	649.3969, 603.3915	Akebia saponin PA[b]	*Radix Dipsaci*
37.04	$[M+HCOO]^-$	301.17961	301.17961	Bakuchiol[b]	*Fructus Psoraleae*

Abbreviations: OVX, ovariectomized; t_R: retention time; XLGB, Xianlinggubao capsule.
[a]Confirmed with reference standards.
[b]Confirmed with MSn fragmentation.
[c]Confirmed with references.[12]

components of XLGB with 328 putative targets, among which 286 target genes were related to the development of OP. Enrichment analysis of KEGG pathway discovered 343 kernel targets and 31 potential pathways ($p < 0.05$), and 19 kernel targets from 28 pathways overlapped with the target compound, confirming their roles in anti-OP effect of XLGB. Then a network with 105 compounds, 19 targets, and 28 pathways was obtained, in which 105 compounds covered all six herbs of XLGB. However, in the compound–target–pathway network, only three compounds were identified in the plasma sample of OVX-OP rats, and this may be attributed to the very low dose of some compounds that could not be detected in this prescription.[12]

Moreover, molecular docking analysis showed 13 compounds (epimedin A, epimedin B, epimedin C, diphylloside B, diphylloside A, icariin, timosaponin B-II, asperosaponin VI, akebiasaponin V, hederagenin-β-sophorosyl ester, olivil-4''-O-β-D-glucopyranoside, 2''-O-rhamnosylicariside II, and 3''-O-Xylopyranosyl epimedoside A) exhibited strong interactions with 14 potential markers (ABL1, CDK2, EGFR, HSP90AA1, HSP90AB1, HSP90B1, MAPK1, NFKB1, NFKB2, NOS2, RB1, SRC, TP53, and VCAM1). Nine of these compounds are from the monarch herb *Herba Epimedii*, three are from the assistant herb *Radix Dipsaci*, and one is from the minister herb *Rhizoma Anemarrhenae*. Our data suggested that the main active compounds in the monarch herbs are flavonoids

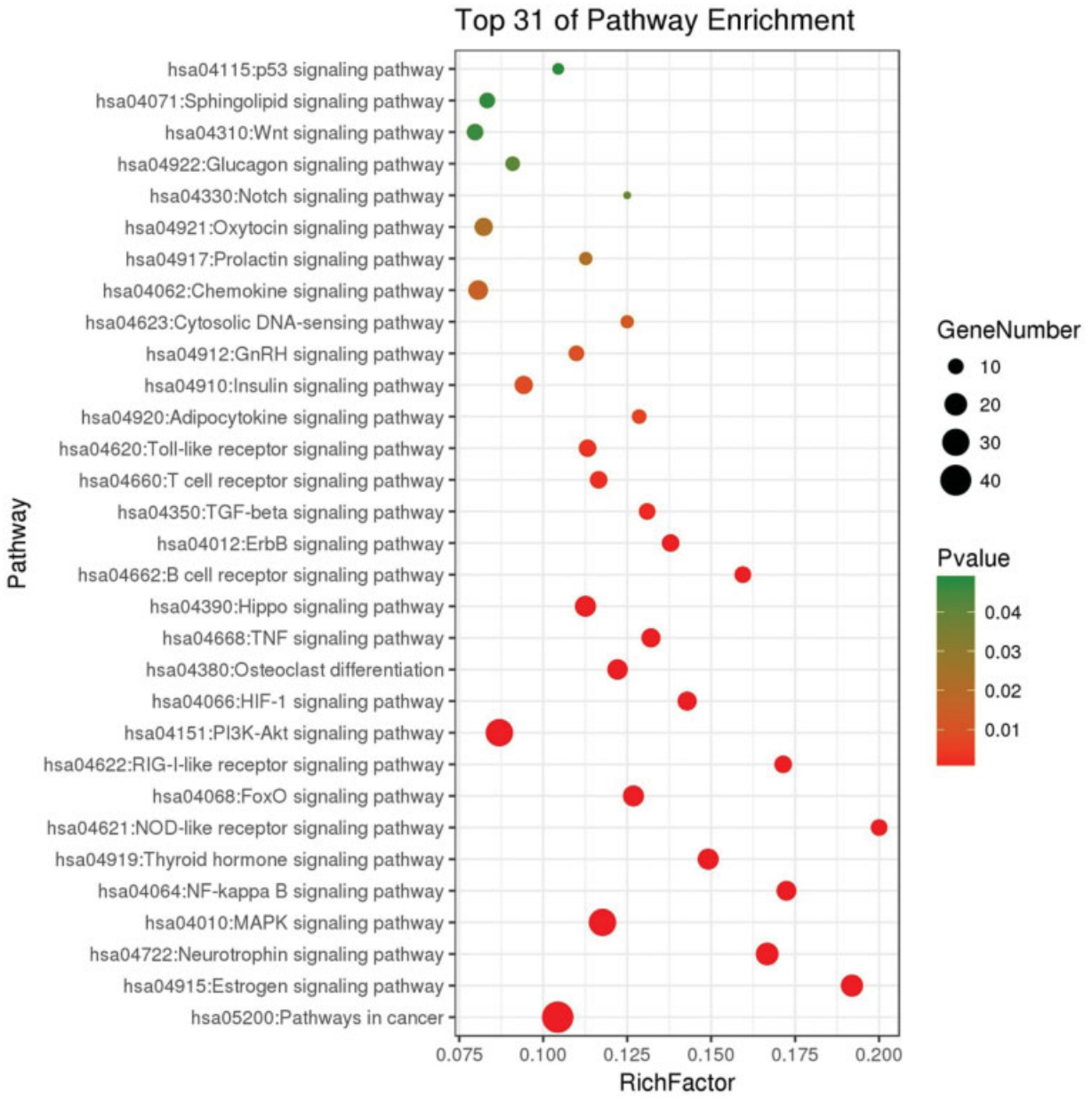

Fig. 4 31 OP-associated pathways with $p \leq 0.05$ through KEGG pathway enrichment. KEGG, Kyoto Encyclopedia of Genes and Genomes; OP, osteoporosis.

and saponins, which make up the most important therapeutic material basis in XLGB. As shown in the absorbed component–potential marker–pathway network, most of the compounds could regulate multiple signaling pathways via multiple targets. For example, epimedin A, epimedin B, and epimedin C (from *Herba Epimedii*) acted on NOS2, CDK2, EGFR, and MAPK1, among which MAPK1 and EGFR are kernel targets in this network, and connect with 22 and 9 signaling pathways, respectively. Timosaponin B-II (from *Rhizoma Anemarrhenae*) was linked to 10 targets and finally acted on 23 pathways. Icariin (from *Herba Epimedii*) connected with 21 pathways through four targets, and has been reported to promote osteogenesis through different pathways including EGFR,[25] MAPK,[26] and PI3K/ATP[27] signaling pathways.

It is worth mentioning that most of the connected 28 pathways in the network were closely related to the development of OP, such as estrogen signaling pathway that usually underlies the anti-OP effect of many TCMs,[28,29] phosphorylation-mediated activation of the MAPK signaling pathway that plays a role in osteoblastic differentiation in mesenchymal cells,[30,31] MAPK signaling molecules (ERK, p38, and JNK) that are related to osteoclast activation, differentiation, and survival,[32,33] PI3K/ATP signaling that is associated with bone tissue metabolism,[34,35] as well as HIF-1 signaling pathway,[36] NF-κB signaling pathway,[37] and Wnt signaling pathway.[38] Some of them (for example the signaling pathway of PI3K-Akt, estrogen, MAPK, ErbB, NOD-like receptor, TNF, and neurotrophin) can be affected by more than five targets.

Table 2 19 potential markers (overlapped kernel targets between the targets of the 31 pathways and the targets of 124 candidate compounds)

NO.	Target name	Description
1	ABL1	Tyrosine-protein kinase ABL1
2	AR	Androgen receptor
3	CDK1	Cyclin-dependent kinase 1
4	CDK2	Cyclin-dependent kinase 2
5	EGFR	Epidermal growth factor receptor
6	ESR1	Estrogen receptor 1
7	HSP90AA1	Heat shock protein HSP 90-α
8	HSP90AB1	Heat shock protein HSP 90-β
9	HSP90B1	Endoplasmin
10	ICAM1	Intercellular adhesion molecule 1
11	JUN	Transcription factor AP-1
12	MAPK1	Mitogen-activated protein kinase 1
13	NFKB1	Nuclear factor NF-kappa-B p105 subunit
14	NFKB2	Nuclear factor NF-kappa-B p100 subunit
15	NOS2	Nitric oxide synthase 2
16	RB1	Retinoblastoma-associated protein
17	SRC	Proto-oncogene tyrosine-protein kinase Src
18	TP53	Cellular tumor antigen p53
19	VCAM1	Vascular cell adhesion protein 1

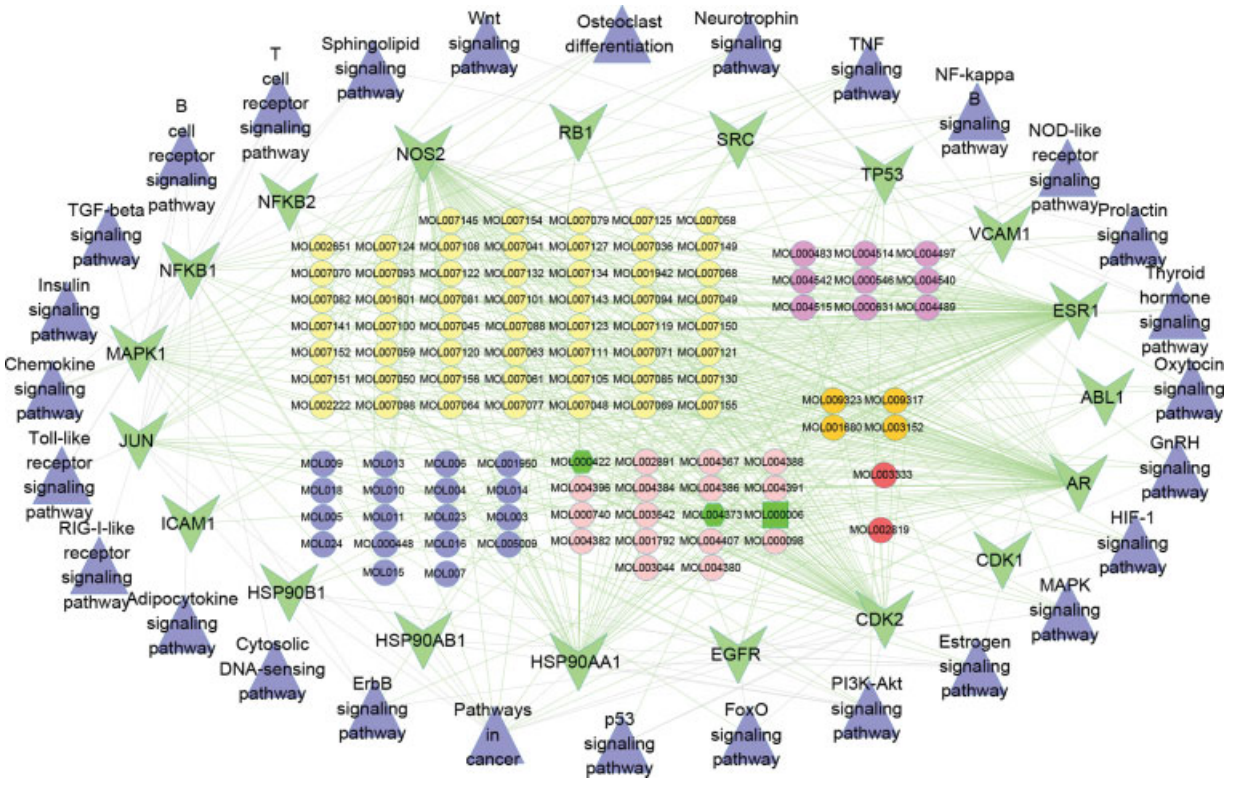

Fig. 5 Compound–target–pathway network (*yellow*, *pink*, *blue*, *purple*, *orange*, and *red circles* stand for compounds of Danshen, Yinyanghuo, Buguzhi, Zhimu, Xuduan, and Dihuang, respectively). *Green V* stands for compound targets. *Blue triangle* stands for pathways. *Emerald green hexagon* stands for common compounds of Zhimu and Yinyanghuo, *Emerald green rectangle* stands for common compounds of Danshen and Yinyanghuo. *Gray lines* stand for interaction among compounds and targets, and *green lines* stand for interaction among targets and pathways).

Table 3 Screened 28 pathways based on KEGG pathway analysis which connected with 19 potential markers

Pathway ID	Pathway description	*p*-Value	Kernel target genes
hsa05200	Pathways in cancer	2.06E − 08	HSP90AB1, TRAF2, GRB2, PML, NFKBIA, NFKB1, NFKB2, PTEN, CTNNB1, AKT1, CUL2, NOS2, TRAF6, MYC, CHUK, FN1, EGFR, AR, HSP90AA1, VHL, RELA, CREBBP, CBL, TP53, SMAD3, SMAD2, RB1, CDK2, MAPK1, CDKN1A, HSP90B1, HDAC2, EP300, HDAC1, JUN, NTRK1, IKBKG, MDM2, ABL1, IKBKB, CRK
hsa04915	Estrogen signaling pathway	4.42E − 08	EGFR, HSP90AB1, HSP90AA1, GRB2, ESR1, HSPA1A, HSPA1B, SRC, HSPA1L, AKT1, MAPK1, HSP90B1, SP1, JUN, CALM3, SHC1, HSPA8, CALM2, CALM1
hsa04722	Neurotrophin signaling pathway	1.86E − 07	GRB2, RELA, TP53, NFKBIA, NFKB1, YWHAE, AKT1, MAPK1, MAP3K3, JUN, NTRK1, MAP3K1, CALM3, SHC1, IKBKB, ABL1, TRAF6, CRK, CALM2, CALM1
hsa04010	MAPK signaling pathway	2.11E − 07	TRAF2, GRB2, NFKB1, HSPA1A, HSPA1B, NFKB2, DAXX, HSPA1L, AKT1, TNFRSF1A, MAP3K3, MAP3K1, TRAF6, MYC, HSPA8, CHUK, EGFR, RELA, TP53, FLNA, MAPK1, ARRB2, ARRB1, NTRK1, JUN, IKBKG, HSPB1, MAP3K14, IKBKB, CRK
hsa04064	NF-kappa B signaling pathway	6.54E − 06	ICAM1, TRAF2, RELA, NFKBIA, NFKB1, UBE2I, NFKB2, VCAM1, TNFRSF1A, CSNK2A1, IKBKG, IKBKB, MAP3K14, TRAF6, CHUK
hsa04919	Thyroid hormone signaling pathway	8.93E − 06	ACTB, KAT2B, CREBBP, TP53, ESR1, SRC, CTNNB1, AKT1, ACTG1, MAPK1, HDAC3, EP300, HDAC2, HDAC1, MDM2, NCOR1, MYC
hsa04621	NOD-like receptor signaling pathway	4.75E − 05	HSP90AB1, MAPK1, HSP90B1, HSP90AA1, RELA, IKBKG, NFKBIA, NFKB1, TRAF6, IKBKB, CHUK
hsa04068	FoxO signaling pathway	6.91E − 05	EGFR, USP7, GRB2, CREBBP, SMAD3, SMAD2, PTEN, SIRT1, CDK2, AKT1, MAPK1, PRMT1, CDKN1A, EP300, MDM2, IKBKB, CHUK
hsa04622	RIG-I-like receptor signaling pathway	8.12E − 05	TRAF2, IKBKE, DDX3X, TBK1, RELA, MAP3K1, IKBKG, NFKBIA, NFKB1, TRAF6, IKBKB, CHUK
hsa04151	PI3K-Akt signaling pathway	8.50E − 05	HSP90AB1, YWHAZ, GRB2, NFKB1, PTEN, CDC37, AKT1, PPP2CA, MYC, CHUK, FN1, EGFR, PPP2R1A, HSP90AA1, RELA, TP53, YWHAB, ITGA4, RPS6, YWHAE, BRCA1, CDK2, MAPK1, CDKN1A, YWHAG, HSP90B1, IKBKG, YWHAQ, MDM2, IKBKB
hsa04066	HIF-1 signaling pathway	1.14E − 04	EGFR, VHL, RELA, CREBBP, NFKB1, RPS6, AKT1, MAPK1, CUL2, CDKN1A, EP300, NOS2, GAPDH, ENO1
hsa04380	Osteoclast differentiation	1.87E − 04	TRAF2, GRB2, RELA, NFKBIA, NFKB1, NFKB2, AKT1, MAPK1, TNFRSF1A, SQSTM1, JUN, IKBKG, IKBKB, MAP3K14, TRAF6, CHUK
hsa04668	TNF signaling pathway	2.53E − 04	ICAM1, TRAF2, RELA, NFKBIA, NFKB1, AKT1, VCAM1, MAPK1, TNFRSF1A, JUN, IKBKG, IKBKB, MAP3K14, CHUK
hsa04662	B cell receptor signaling pathway	3.39E − 04	AKT1, MAPK1, GRB2, JUN, RELA, CD81, IKBKG, NFKBIA, NFKB1, IKBKB, CHUK
hsa04012	ErbB signaling pathway	5.80E − 04	AKT1, EGFR, MAPK1, CDKN1A, GRB2, JUN, CBL, SHC1, ABL1, CRK, MYC, SRC
hsa04350	TGF-β signaling pathway	1.64E − 03	MAPK1, PPP2R1A, EP300, SP1, PPP2CA, CREBBP, SMAD3, SMAD2, SMURF1, MYC, CUL1
hsa04660	T cell receptor signaling pathway	2.36E − 03	AKT1, MAPK1, GRB2, JUN, RELA, CBL, IKBKG, NFKBIA, NFKB1, MAP3K14, IKBKB, CHUK
hsa04620	Toll-like receptor signaling pathway	2.97E − 03	AKT1, MAPK1, IKBKE, TBK1, JUN, RELA, IKBKG, NFKBIA, NFKB1, TRAF6, IKBKB, CHUK
hsa04920	Adipocytokine signaling pathway	6.04E − 03	AKT1, TRAF2, TNFRSF1A, RELA, IKBKG, NFKBIA, NFKB1, IKBKB, CHUK
hsa04910	Insulin signaling pathway	8.20E − 03	AKT1, MAPK1, PPP1CA, GRB2, CBL, CALM3, SHC1, IKBKB, PPP1CC, RPS6, CRK, CALM2, CALM1
hsa04912	GnRH signaling pathway	9.47E − 03	EGFR, MAPK1, MAP3K3, GRB2, JUN, MAP3K1, CALM3, SRC, CALM2, CALM1
hsa04623	Cytosolic DNA-sensing pathway	1.26E − 02	IKBKE, TBK1, RELA, IKBKG, NFKBIA, NFKB1, IKBKB, CHUK
hsa04062	Chemokine signaling pathway	1.51E − 02	GRB2, RELA, NFKBIA, NFKB1, PXN, SRC, AKT1, MAPK1, ARRB2, ARRB1, IKBKG, SHC1, IKBKB, CRK, CHUK
hsa04917	Prolactin signaling pathway	2.14E − 02	AKT1, MAPK1, GRB2, RELA, ESR1, NFKB1, SHC1, SRC
hsa04921	Oxytocin signaling pathway	2.22E − 02	ACTB, EGFR, EEF2, PPP1CC, SRC, ACTG1, MAPK1, PPP1CA, CDKN1A, JUN, CALM3, CALM2, CALM1
hsa04310	Wnt signaling pathway	4.60E − 02	CSNK2A1, EP300, BTRC, JUN, CREBBP, TP53, RUVBL1, MYC, FBXW11, CUL1, CTNNB1
hsa04071	Sphingolipid signaling pathway	4.74E − 02	AKT1, MAPK1, PPP2R1A, TRAF2, TNFRSF1A, PPP2CA, RELA, TP53, NFKB1, PTEN
hsa04115	p53 signaling pathway	4.81E − 02	CDK1, CDKN1A, TP53, MDM2, SFN, PTEN, CDK2

Abbreviation: KEGG, Kyoto Encyclopedia of Genes and Genomes.

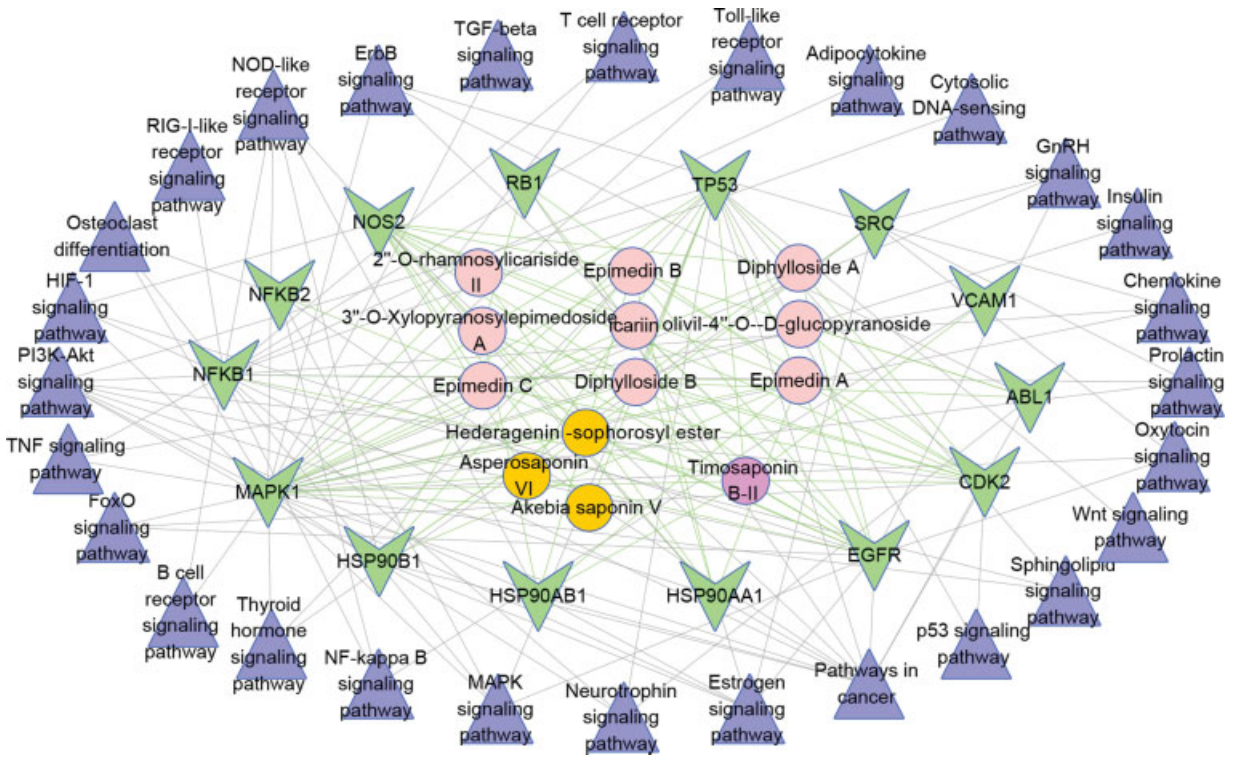

Fig. 6 Absorbed component–potential marker–pathway network (*pink*, *purple*, and *orange circles* stands for compounds of Yinyanghuo, Zhimu, Xuduan, respectively). *Green V* stands for potential targets. *Blue triangle* stands for pathways. *Gray lines* stand for interaction between targets and pathways. *Green lines* stand for interaction between targets and compounds.

Conclusions

Our study was in accordance with traditional Chinese medicine theory and the *multicomponent, multitarget*, and *multipathway* characteristics of TCM. We investigated the possible active compounds of XLGB and the underlying therapeutic mechanisms from a systemic perspective. Our data provided a strong link between the major active components and potential targets, helped to delineate the anti-OP effect of XLGB and guide of the deconvolution of therapeutic effects of multi-component herbal treatment.

Author Contributions

Xiao Hu designed the experiments and checked the final manuscript. Yun-Hui Xu performed the experiments, analyzed and interpreted the results, and wrote the manuscript. Yi-Chun Sun performed some experiments, contributed materials, and checked the data. Jie Liu searched the relevant literature. Hui-Xin Li, Chun-Yue Huang, and Yuan-Yuan Pang provided helpful discussions. Tong Wu directed the research. All authors have read and approved the final version of this manuscript.

Funding Statement

This research was funded by the Project of Standardization of Chinese Materia Medica (Grant No. ZYBZH-C-GZ-10), China Postdoctoral Science Foundation (Grant No. 2018M633022), and National Science and Technology Major Project (Grant No. 2018ZX09731-016).

Conflicts of Interest

The authors declare no conflict of interest.

Acknowledgments

We thank Guangzhou Yinfo Information Technology Co. Ltd. for providing an easy and versatile Dock Web App to aid the docking studies.

References

1 Awasthi H, Mani D, Singh D, Gupta A. The underlying pathophysiology and therapeutic approaches for osteoporosis. Med Res Rev 2018;38(06):2024–2057
2 Madrasi K, Li F, Kim MJ, et al. Regulatory perspectives in pharmacometric models of osteoporosis. J Clin Pharmacol 2018;58(05):572–585
3 Burge R, Dawson-Hughes B, Solomon DH, Wong JB, King A, Tosteson A. Incidence and economic burden of osteoporosis-related fractures in the United States, 2005-2025. J Bone Miner Res 2007;22(03):465–475
4 Chen P, Li Z, Hu Y. Prevalence of osteoporosis in China: a meta-analysis and systematic review. BMC Public Health 2016;16(01):1039
5 Mithal A, Bansal B, Kyer CS, Ebeling P. The Asia-Pacific regional audit-epidemiology, costs, and burden of osteoporosis in India 2013: a report of International Osteoporosis Foundation. Indian J Endocrinol Metab 2014;18(04):449–454
6 Cooper C, Cole ZA, Holroyd CR, et al; IOF CSA Working Group on Fracture Epidemiology. Secular trends in the incidence of hip and other osteoporotic fractures. Osteoporos Int 2011;22(05):1277–1288
7 Liu K, Tan LJ, Wang P, et al. Functional relevance for associations between osteoporosis and genetic variants. PLoS One 2017;12(04):e0174808

8 Liu Y, Liu JP, Xia Y. Chinese herbal medicines for treating osteoporosis. Cochrane Database Syst Rev 2014;6(03):CD005467
9 Zhu HM, Qin L, Garnero P, et al. The first multicenter and randomized clinical trial of herbal Fufang for treatment of postmenopausal osteoporosis. Osteoporos Int 2012;23(04):1317–1327
10 Qin L, Zhang G, Hung WY, et al. Phytoestrogen-rich herb formula "XLGB" prevents OVX-induced deterioration of musculoskeletal tissues at the hip in old rats. J Bone Miner Metab 2005;23 (Suppl):55–61
11 State Food and Drug Administration of China Xianlinggubao Capsule, WS-10269 (ZD-0269)-2002. National Standards Assembly of Chinese Patent Medicine, 2002.
12 Dai Y, Tu FJ, Yao ZH, et al. Rapid identification of chemical constituents in traditional Chinese medicine fufang preparation xianling gubao capsule by LC-linear ion trap/Orbitrap mass spectrometry. Am J Chin Med 2013;41(05):1181–1198
13 Bao H, Guo H, Feng Z, Li X. Deciphering the underlying mechanism of Xianlinggubao capsule against osteoporosis by network pharmacology. BMC Complement Med Ther 2020;20(01):208
14 Lee AY, Park W, Kang TW, Cha MH, Chun JM. Network pharmacology-based prediction of active compounds and molecular targets in Yijin-Tang acting on hyperlipidaemia and atherosclerosis. J Ethnopharmacol 2018;221:151–159
15 Cheng M, Wang Q, Fan Y, et al. A traditional Chinese herbal preparation, Er-Zhi-Wan, prevent ovariectomy-induced osteoporosis in rats. J Ethnopharmacol 2011;138(02):279–285
16 Bahlous A, Kalai E, Hadj Salah M, Bouzid K, Zerelli L. Biochemical markers of bone remodeling: recent data of their applications in managing postmenopausal osteoporosis [in French]. Tunis Med 2006;84(11):751–757
17 Lei T, Liang Z, Li F, et al. Pulsed electromagnetic fields (PEMF) attenuate changes in vertebral bone mass, architecture and strength in ovariectomized mice. Bone 2018;108:10–19
18 Lipinski CA. Lead- and drug-like compounds: the rule-of-five revolution. Drug Discov Today Technol 2004;1(04):337–341
19 Ru J, Li P, Wang J, et al. TCMSP: a database of systems pharmacology for drug discovery from herbal medicines. J Cheminform 2014;6:13
20 Huang W, Sherman BT, Lempicki RA. Systematic and integrative analysis of large gene lists using DAVID bioinformatics resources. Nat Protoc 2009;4(01):44–57
21 Lang PT, Brozell SR, Mukherjee S, et al. DOCK 6: combining techniques to model RNA-small molecule complexes. RNA 2009;15(06):1219–1230
22 Missiuro PV, Liu K, Zou L, et al. Information flow analysis of interactome networks. PLOS Comput Biol 2009;5(04):e1000350
23 Tang Y, Li M, Wang J, Pan Y, Wu FX. CytoNCA: a cytoscape plugin for centrality analysis and evaluation of protein interaction networks. Biosystems 2015;127:67–72
24 Geng JL, Dai Y, Yao ZH, et al. Metabolites profile of Xian-Ling-Gu-Bao capsule, a traditional Chinese medicine prescription, in rats by ultra performance liquid chromatography coupled with quadrupole time-of-flight tandem mass spectrometry analysis. J Pharm Biomed Anal 2014;96:90–103
25 Zhang D, Liu L, Jia Z, Yao X, Yang M. Flavonoids of Herba Epimedii stimulate osteogenic differentiation and suppress adipogenic differentiation of primary mesenchymal stem cells via estrogen receptor pathway. Pharm Biol 2016;54(06):954–963
26 Wu Y, Xia L, Zhou Y, Xu Y, Jiang X. Icariin induces osteogenic differentiation of bone mesenchymal stem cells in a MAPK-dependent manner. Cell Prolif 2015;48(03):375–384
27 Zhai YK, Guo XY, Ge BF, et al. Icariin stimulates the osteogenic differentiation of rat bone marrow stromal cells via activating the PI3K-AKT-eNOS-NO-cGMP-PKG. Bone 2014;66:189–198
28 You L, Chen L, Pan L, Chen JY. New insights into the gene function of osteoporosis. Front Biosci 2013;18:1088–1097
29 Xu F, Ding Y, Guo Y, et al. Anti-osteoporosis effect of Epimedium via an estrogen-like mechanism based on a system-level approach. J Ethnopharmacol 2016;177:148–160
30 Higuchi C, Myoui A, Hashimoto N, et al. Continuous inhibition of MAPK signaling promotes the early osteoblastic differentiation and mineralization of the extracellular matrix. J Bone Miner Res 2002;17(10):1785–1794
31 Peng S, Zhou G, Luk KD, et al. Strontium promotes osteogenic differentiation of mesenchymal stem cells through the Ras/MAPK signaling pathway. Cell Physiol Biochem 2009;23(1-3):165–174
32 David JP, Sabapathy K, Hoffmann O, Idarraga MH, Wagner EF. JNK1 modulates osteoclastogenesis through both c-Jun phosphorylation-dependent and -independent mechanisms. J Cell Sci 2002; 115(Pt 22):4317–4325
33 Ikeda F, Nishimura R, Matsubara T, et al. Critical roles of c-Jun signaling in regulation of NFAT family and RANKL-regulated osteoclast differentiation. J Clin Invest 2004;114(04):475–484
34 Xi JC, Zang HY, Guo LX, et al. The PI3K/AKT cell signaling pathway is involved in regulation of osteoporosis. J Recept Signal Transduct Res 2015;35(06):640–645
35 Ke K, Li Q, Yang X, et al. Asperosaponin VI promotes bone marrow stromal cell osteogenic differentiation through the PI3K/AKT signaling pathway in an osteoporosis model. Sci Rep 2016; 6:35233
36 Zhong H, Cao C, Yang J, Huang Q. Research on Relationship of HIF-1 Signaling Pathway and Postmenstrual Osteoporosis [in Chinese]. Sichuan Da Xue Xue Bao Yi Xue Ban 2017;48(06):862–868
37 Xu Q, Chen G, Liu X, Dai M, Zhang B. Icariin inhibits RANKL-induced osteoclastogenesis via modulation of the NF-κB and MAPK signaling pathways. Biochem Biophys Res Commun 2019;508(03):902–906
38 Amjadi-Moheb F, Akhavan-Niaki H. Wnt signaling pathway in osteoporosis: Epigenetic regulation, interaction with other signaling pathways, and therapeutic promises. J Cell Physiol 2019; 234(09):14641–14650